中国光学（中英文） Chinese Optics 核心期刊

高波前拟合精度的紧凑型音圈变形镜

胡立发 姜律 胡启立 徐星宇 黄杨 吴晶晶 俞琳

Compact voice coil deformable mirror with high wavefront fitting precision

HU Li-fa, JIANG Lv, HU Qi-li, XU Xing-yu, HUANG Yang, WU Jing-jing, YU Lin

引用本文:
胡立发, 姜律, 胡启立, 徐星宇, 黄杨, 吴晶晶, 俞琳. 高波前拟合精度的紧凑型音圈变形镜[J]. 中国光学, 2023, 16(6): 1463-1474. doi: 10.37188/CO.EN-2023-0001
HU Li-fa, JIANG Lv, HU Qi-li, XU Xing-yu, HUANG Yang, WU Jing-jing, YU Lin. Compact voice coil deformable mirror with high wavefront fitting precision[J]. *Chinese Optics*, 2023, 16(6): 1463-1474. doi: 10.37188/CO.EN-2023-0001

在线阅读 View online: https://doi.org/10.37188/CO.EN-2023-0001

文章编号 2097-1842(2023)06-1463-12

Compact voice coil deformable mirror with high wavefront fitting precision

HU Li-fa[1,3], JIANG Lv[1,3], HU Qi-li[2], XU Xing-yu[1,3], HUANG Yang[1,3*], WU Jing-jing[1,3], YU Lin[1,3]
(1. *School of Science*, *Jiangnan University*, *Wuxi* 214122, *China*;
2. *Key Laboratory of Electro-Optical Countermeasures Test & Evaluation Technology*, *Luoyang* 471003, *China*;
3. *Jiangsu Provincial Research Center of Light Industrial Opto-electronic Engineering and Technology*, *Wuxi* 214122, *China*)
* *Corresponding author*, *E-mail*: *yanghuang@jiangnan.edu.cn*

Abstract: To meet the requirements of wavefront distortion correction for miniaturized adaptive optics systems, a Deformable Mirror (DM) using micro voice coil actuators was designed based on systematic theoretical analysis. The structural parameters of the micro voice coil actuator were optimized by electromagnetic theory and the finite element method. The DM was optimized with respect to thermal deformation, resonance frequency, coupling coefficient and other parameters. Finally, wavefront fitting and residual calculation were completed according to the influence function. The optimized 69-element Voice Coil Deformable Mirror (VCDM) has a large phase stroke, good thermal stability, and a large first resonance of 2220 Hz. The RMS of the fitting residuals of the VCDM for the first 35 Zernike modes with a PV value of 1 μm are all below 30 nm. For complex random aberrations, the compact VCDM can reduce the wavefront RMS to less than 10%. Compared with a traditional VCDMs, the results of our compact VCDM indicate that it has a higher wavefront fitting precision. The compact VCDM with high performance and low cost has good potential applications in human retinal or airborne imaging systems.

Key words: adaptive optics; deformable mirror; voice coil actuator; multiparameter analysis

高波前拟合精度的紧凑型音圈变形镜

胡立发[1,3], 姜 律[1,3], 胡启立[2], 徐星宇[1,3], 黄 杨[1,3*], 吴晶晶[1,3], 俞 琳[1,3]
(1. 江南大学 理学院, 江苏 无锡 214122;
2. 光电对抗测试与评估重点实验室, 河南 洛阳 471003;
3. 江苏省轻工光电工程技术研究中心, 江苏 无锡 214122)

摘要: 为了满足小型化自适应光学系统校正波前畸变的需求, 基于系统理论分析设计了一种使用微型音圈驱动器的变形

收稿日期: 2023-01-10; **修订日期:** 2023-03-09
基金项目: 国家自然科学基金 (No. 61475152); 光电对抗测试与评估重点实验室开放基金 (No. GKCP2021001)
Supported by National Natural Science Foundation of China (No. 61475152); Fund for Key Laboratory of Electro-Optical Countermeasures Test & Evaluation Technology (No. GKCP2021001)

镜。使用电磁理论和有限元方法优化了微型音圈驱动器的结构参数。从热变形、共振频率、耦合系数等多个参数的角度对变形镜进行了优化。最后根据影响函数完成了波前拟合和残差计算。优化后的 69 单元紧凑型音圈变形镜具有大相位调制量、良好的热稳定性，第一共振频率为 2 220 Hz。对于 PV 值为 1 μm 的前 35 项泽尼克模式，紧凑型音圈变形镜的拟合残差均小于 30 nm。对于复杂随机像差，紧凑型 VCDM 能够将波前 RMS 降至原来的 10% 以下。结果表明，与传统的音圈变形镜相比，紧凑型音圈变形镜具有更高的波前拟合精度。高性能、低成本的紧凑型音圈变形镜在视网膜成像和机载成像系统中具有良好的应用前景。

关 键 词: 自适应光学；变形镜；音圈驱动器；多参数分析

中图分类号: TH74 **文献标志码:** A **doi:** 10.37188/CO.EN-2023-0001

1 Introduction

In adaptive optical imaging systems, the Deformable Mirror (DM) is usually used to correct aberrations induced by atmospheric turbulence[1]. Different kinds of DMs have been investigated, such as the piezoelectric (PZT) DM[2], magnetic fluid DM[3], electrostatic DM[4], and voice coil DM (VCDM)[5]. Compared with others, the VCDM has many merits, such as linear responses, a large phase stroke, and low voltage, which is suitable for the next generation of DMs with research spanning back to the 1990 s[6].

In 1993, P. Salinari demonstrated a VCDM as a deformable secondary mirror of the Large Binoculars Telescope (LBT). After that, a prototype of P36 was manufactured and demonstrated based on the principle. The MMT336 DM was fabricated in 2000 and installed on the Multi-mirror Telescope (MMT) in 2002[7]. MMT was the first ground-based optical telescope equipped with a VCDM as the adaptive secondary mirror, followed by the Large Binoculars Telescope, the Magellan Telescope, the Very Large Telescope, and others[8]. However, the diameter of a Voice Coil Actuator (VCA) in these DMs ranges between 20 mm and 30 mm, which leads to a large VCDM with an aperture of about 1 000 mm. Large VCAs also require cooling systems. In addition, its coupling coefficient is generally larger than 60%, which is much larger than that of PZT-based DM. For a compact VCDM, a relatively small coupling coefficient is valuable to obtain high wavefront correction precision. Finally, it should be noted that it is expensive to use custom VCDMs with complex structures. In applications, such as retinal imaging, biological microscopy, and optical communications, a compact and relatively inexpensive DM with high electro-optical performance is necessary.

Several kinds of compact DMs have been investigated, such as the membrane DM[9], micro-electro-mechanical system (MEMS) DM[10], and magnetic DM[11]. The membrane DM is composed of a flexible silicon membrane supported by an underlying array of electrostatic parallel plate actuators. Usually, its phase stoke is not large, and its driving voltage is relatively high at about several tens of volts[12]. In addition, a dedicated electronic device is needed to linearize its actuation. Although the MEMS DM has a large number of actuators, its phase stroke is only about several micrometers[13], limiting its applications as a wavefront corrector in adaptive optics systems. The magnetic DM uses small planar coils on silicon. Therefore, to generate large enough force to push or pull in the thin mirror of a magnetic DM, a relatively large current is necessary, which leads to high power dissipation. VCDMs have the merits of low cost and linear response compared to PZT DM. However, standard VCDMs have two obvious drawbacks: (1) large coil diameters with a high cost and relatively low bandwidth, (2) high coupling coefficient and a large current that cannot be used in a compact VCDM. Multiple compact VCDMs from ALPAO have a pitch of 0.8 mm, 1.5 mm, 2.5 mm, and 5 mm, and the number of actuators ranges from 69 to 3 228. They have a non-linearity below 3%, and a hysteresis as low as 2%. However, these VCDMs use the MEMS manufacturing process resulting in high costs. In this pa-

per, an alternative compact VCDM is presented by deriving theoretical equations that could guide a reasonable design. The designed micro VCA has a small diameter of about 2 mm, which is only about a tenth of a standard one and allows a compact VCDM with a high density of actuators. Different factors such as phase stroke, resonant frequency, and power dissipation were analyzed. The VCDM's structure has been simplified and optimized to realize a low coupling coefficient and good electro-optical performances. In fact, these parameters are influenced by the interactions among multi-physical fields, such as electromagnetic, thermal, stress and strain fields. For example, increasing the current in a voice coil can produce a large electromagnetic force and increase its phase stroke. However, it can also lead to a large thermal dissipation, and even distort the VCDM's thin mirror. Therefore, theoretical mathematical equations were derived to find reasonable requirements from applications. Further, numerical simulations based on the finite element method were used to optimize the compact VCDM.

In the paper, the compact VCDM with high electro-optical performance is theoretically designed and demonstrated. In section 2, a theoretical analysis is given according to their typical applications. In section 3, its structure is designed, and its micro VCA is optimized based on electromagnetic finite element theory. In section 4, the temporal and spatial properties of the compact VCDM using optimized micro VCA are discussed. Finally, conclusions are given in section 5.

2　Theory of the compact VCDM

There are many factors that affect the electro-optical performance of a compact VCDM, such as phase stroke, the electromagnetic force of the micro VCA, the power dissipation and efficiency of the micro VCA, the response time of the VCDM and the coupling coefficient. A DM with only one or two of them with excellent values as reported in the references could not really lead to a high electro-optical performance for a compact VCDM[5]. Therefore, it is necessary to systematically analyze the requirements from the applications according to electromagnetic theory.

2.1　Requirement of phase stroke and frequency for the VCDM

The phase stroke of the VCDM is determined by the stroke of its micro VCA. The phase stroke requirement of a DM could be different according to the media that the light beam propagates through, such as atmospheric turbulence or the human eye. For airborne/spaceborne adaptive optics applications, according to Noll's theory, if the first J Zernike modes of the distortion have been corrected, the mean square residual error can be calculated as follows:

$$\Delta_J = \langle \phi^2 \rangle - \sum_{j=1}^{J} \langle |a_j|^2 \rangle \quad , \qquad (1)$$

where $\langle \phi^2 \rangle$ is the phase variance and a_j is the Zernike polynomial coefficient[14]. When J is 1, Eq. (1) can be approximated as

$$\Delta_1 = 1.029\,9\left(\frac{D}{r_0}\right)^{5/3} \quad , \qquad (2)$$

where D is the telescope aperture and r_0 is the atmospheric turbulence coherent length generally ranging from 5 cm to 20 cm for λ=550 nm[15]. For an r_0 of 5 cm and D of 8.4 m, Δ_1 is equal to 5 268 rad^2 according to Eq. (2). The wavefront that the DM has to correct is about 5 times larger than the residual[16]. In addition, considering the reflection doubling effect, the required mechanical stroke of a VCA for atmospheric turbulence correction could be calculated as

$$S_a = \frac{\lambda}{2\pi} \times 5 \times \frac{\sqrt{\Delta_1}}{2} \approx 15.89\,\mu m \quad . \qquad (3)$$

Unlike the aberrations of atmospheric turbulence, those in the human eye are difficult to represent using a theoretical model. Therefore, we take the approximate requirements for the phase stroke from experimental statistical results reported by other

groups. Doble N[17] measured human eye aberrations on two different populations at the University of Rochester and Indiana University using a Shack-Hartmann wavefront sensor. The maximum PV of the wavefront is up to 53 μm for a pupil diameter ranging from 2 mm to 7.5 mm. Zhao J L[18] performed an aberration analysis on 332 healthy eyes and 344 diseased eyes. For a wavelength of 550 nm and a pupil diameter of 6 mm, the PV value of the total-order aberrations was (24.1±10.9) μm in the normal group and (19.0±10.05) μm in the abnormal group[18]. Therefore, the mechanical phase stroke of a micro VCA should be at least 26.5 μm for human eye aberration correction.

According to the discussions above, retinal imaging requires a larger phase stroke compared to astronomical observation. Considering the static aberration in the optical path, the compact VCDM needs a margin of phase modulation. The phase stroke of the compact VCDM should be at least 27 μm.

The bandwidth of the VCDM should be high enough to meet the frequency of atmospheric turbulence aberrations[19]. The Greenwood frequency is usually used to characterize atmospheric turbulence and it could be approximated as:

$$f_c = 0.43\frac{v}{r_0} \quad . \tag{4}$$

where v is the wind speed, and r_0 is the atmospheric turbulence coherence length. And the Greenwood frequency in an observatory station is necessarily larger than 50 Hz.

2.2 Key parameters of micro VCA

The electromagnetic force generated by the micro VCA directly determines the phase stroke of the VCDM[20]. A micro VCA as shown in Fig.1. includes mainly two parts: one is the permanent magnet on the top and the other is the voice coil. When a current is passed through the voice coil, the magnet connected to the thin mirror of the DM is movable, which pushes or pulls the local thin mirror and generates deformation.

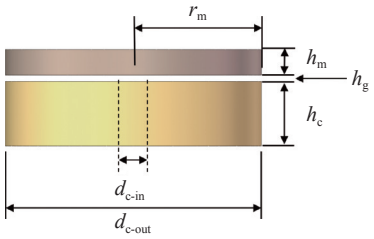

Fig. 1 Structure of micro VCA

In Fig.1, r_m is the magnet's radius, h_m is its height, $d_{c\text{-}in}$ is the coil's inner diameter, $d_{c\text{-}out}$ is the coil's outer diameter, h_c is the coil's height, and h_g is the height of the air gap. When the permanent magnet in the VCA is in the magnetic field generated by the current-carrying coil, the electromagnetic force could be calculated as

$$F = \int_V B_r \nabla \boldsymbol{H} \mathrm{d}v = \int_V B_r \nabla \int_L \frac{1}{4\pi} \frac{\mathrm{Id}\boldsymbol{l} \times \boldsymbol{e}_r}{\boldsymbol{r}^2} \mathrm{d}v \quad , \tag{5}$$

where V is the volume of a permanent magnet, and B_r is the remanence of the permanent magnet, $\boldsymbol{H}$ is field vector, Id$\boldsymbol{l}$ is the current element, and $\boldsymbol{e}_r$ is unit vector along a position vector $\boldsymbol{r}$. Eq. (5) connects the force to some important parameters such as the material and direction of a magnet, the current, the geometric size of the coil, and the gap h_g. The finite element method is used to simulate the electric-magnetic field and calculate the force.

To quantify analyze the performance of the micro VCA, efficiency ε is used as the evaluation factor[21]. It could be calculated as

$$\varepsilon = \frac{F}{\sqrt{I^2 R}} = \int_V B_r \cdot \nabla \int_L \frac{1}{4\pi} \frac{\mathrm{d}\boldsymbol{l} \times \boldsymbol{e}_r}{\boldsymbol{r}^2 \sqrt{\mathrm{R}}} dv, \tag{6}$$

where the unit of ε is N/$\sqrt{\mathrm{W}}$, F is the electromagnetic force, I is the current through the coil, and R is the resistance of the coil. The larger the efficiency of the VCA, the better it is.

3 Design and optimization of the compact VCDM

The sectional view of the compact VCDM is shown in Fig.2(a). The structure of compact VCDM mainly includes ten components. The pupil diameter in the front shell is 17 mm. Fig.2(b) shows the ar-

rangement of VCAs. Sixty-nine VCAs are arranged in a square array under the thin mirror. A single micro VCA contains a permanent magnet and a voice coil. One end of the strut is attached to a micro VCA, while the other is attached to the back of the thin mirror. The strut transmits the force of an actuator to the thin mirror and deforms the local surface of the thin mirror. The shaft of a strut is mounted with a spring in the spring-fixing plate. This structure provides the micro VCA with axial stiffness, which overcomes the problem where an actuator's mover is directly suspended on the mirror in traditional VCDMs[22]. The thin mirror is formed by spinning and depositing polyimide liquid on a highly smooth substrate. The assembly process of the DM can be found in reference [16].

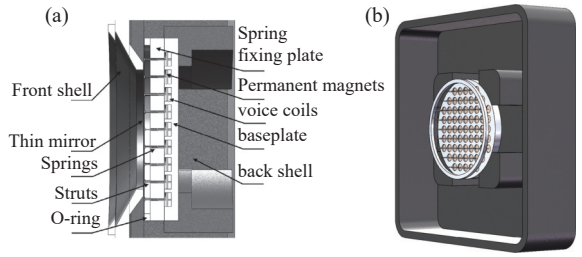

Fig. 2　Structure of VCDM. (a) Sectional view; (b) arrangement of VCAs

To realize the compact VCDM, the pitch of actuators must be small enough. The geometrical shape of the VCA array as shown in Fig.2 is square with a pitch of 2.5 mm. To ensure that there is an installation gap between the actuators, the diameter of a VCA should not be greater than 2.2 mm. At the same time, the mover of the VCA should be as small as possible to get a faster response, so the initial height of the magnet is set to 0.1 mm. The geometrical model of the VCAs is built and simulated with FEM. The initial geometrical sizes for the micro VCA are defined as follows: (1) a permanent magnet with a radius of 1 mm and a height of 0.1 mm; (2) a coil with an inner diameter of 0.2 mm, an outer diameter of 2.2 mm, and a height of 1 mm. To meet the phase stroke requirements calculated in Section 2.1 and reserve redundancy, the initial size of the air gap is set to 50 μm. The permanent magnet is made of NdFe35. The parameters that need to be optimized are listed in Tab. 1.

Tab. 1　Parameters for micro VCAs to be optimized

Parameters	Values(mm)	Step
Magnet radius r_m	$0.1 \leqslant r_m \leqslant 1.1$	0.1
Magnet height h_m	$0.05 \leqslant h_m \leqslant 1$	0.05
Coil inner diameter $d_{c\text{-}in}$	$0.2 \leqslant d_{c\text{-}in} \leqslant 1$	0.2
Coil outer diameter $d_{c\text{-}out}$	$0.4 \leqslant d_{c\text{-}out} \leqslant 2.2$	0.2
Coil height h_c	$0.1 \leqslant h_c \leqslant 1$	0.1
Air gap h_g	$50 \leqslant h_g \leqslant 100$	10

In our previous work[21], for axial and radial magnetization directions of the permanent magnet shown in Fig.3(a) and 3(c), the outputted force generated by radial magnetization must be larger than that of the axial magnetization. However, it is difficult to realize radial magnetization for the permanent magnet with so small a size. In addition, parallel magnetization as shown in Fig.3(b) is easy to achieve.

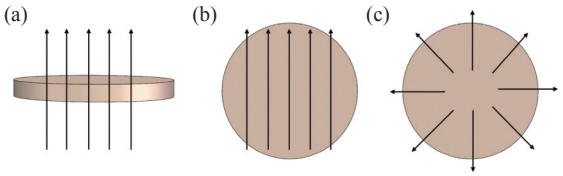

Fig. 3　Magnetization directions of the permanent magnet. (a) Axial magnetization, (b) parallel magnetization, (c) radial magnetization

Fig.4 (color online) shows the comparison of electromagnetic force in three magnetization direc-

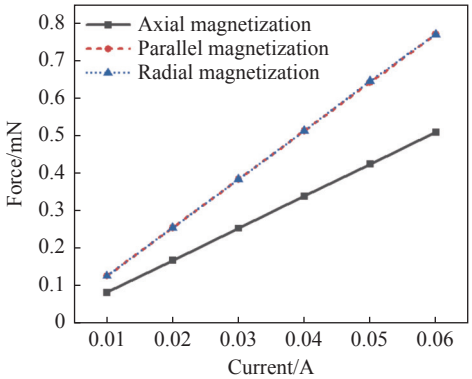

Fig. 4　Electromagnetic force as a function of current for the permanent magnet at different magnetization directions

tions. From Fig.4 It can be seen that the effect of parallel magnetization is very good, and the electromagnetic force under the same current is close to that of radial magnetization.

Fig.5 (color online) shows the optimization results of the structural parameters under parallel magnetization and radial magnetization where parallel magnetization is represented as (P) radial magnetization as (R).

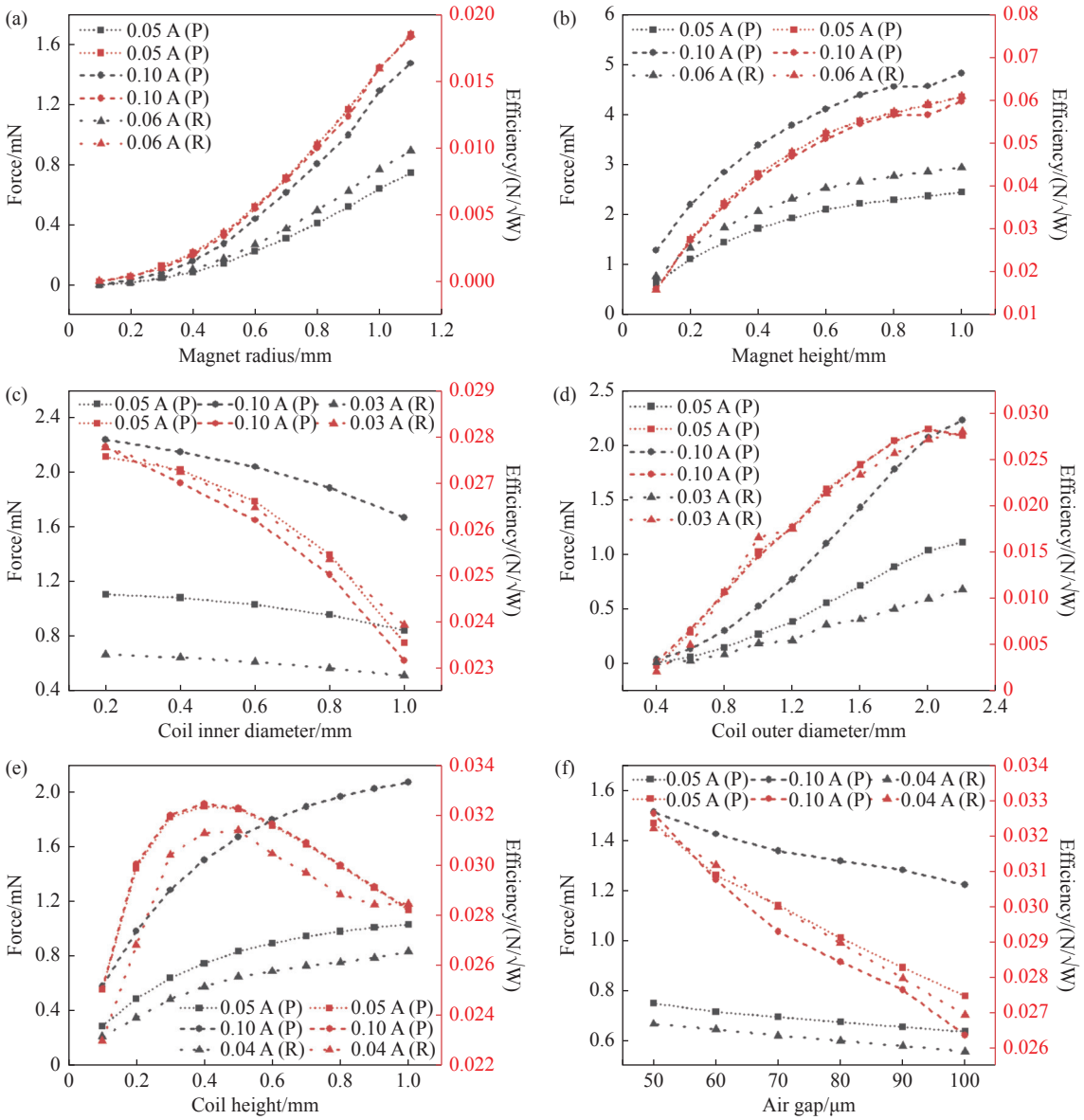

Fig. 5 Force and efficiency as a function of the VCA's structural parameters: (a) permanent magnet radius; (b) permanent magnet height; (c) coil inner diameter; (d) coil outer diameter; (e) coil height; (f) air gap

Fig.5(a) and Fig.5(b) show the electromagnetic force and efficiency ε as a function of magnet radius and height, respectively. The trade-off between efficiency and size is what determines the parameters. The larger the magnet radius and magnet height, the larger the electromagnetic force and efficiency. Their differences are the slopes of the electromagnetic force and efficiency curves. It should be noted that the permanent magnet is the determinant of the VCA, and increasing the permanent magnet's volume will reduce the response speed of the VCA. Therefore, the optimized radius of the magnet is selected as 1 mm and its optimized height is selected as 0.2 mm. The results in Fig.5(c) indicate that as

the inner diameter of the coil increases, both the electromagnetic force and the efficiency decrease. The optimized inner diameter of the coil is 0.2 mm and according to Fig.5(d), the optimized outer diameter of the coil is 2 mm. The change of force and efficiency in Fig.5(e) are slightly different from the others. Although the electromagnetic force increases with the height of the coil, its efficiency first increases and then decreases. This is because the wire being far away from the permanent magnet means that it contributes less to the electromagnetic force. Considering the efficiency of the actuator, the optimized coil height is 0.4 mm. Fig.5(f) shows that the larger the air gap, the smaller the electromagnetic force and efficiency. Therefore, the optimized air gap of the micro VCA is 50 μm.

The optimized VCA has a diameter of 2 mm and a height of 0.65 mm. It is only one-tenth the size of the actuators for traditional VCDMs. Fig.6 (color online) shows electromagnetic force and efficiency as a function of current before and after optimization. The obtained results indicate that the electromagnetic force and efficiency increased substantially after optimization. The output electromagnetic force of the VCA with optimized structural parameters increased by a factor of 10%. The results confirm that the efficiency also notably increased. The efficiency of the VCA before optimization is 0.016 N/√W and it is up to 0.032 N/√W after optimization.

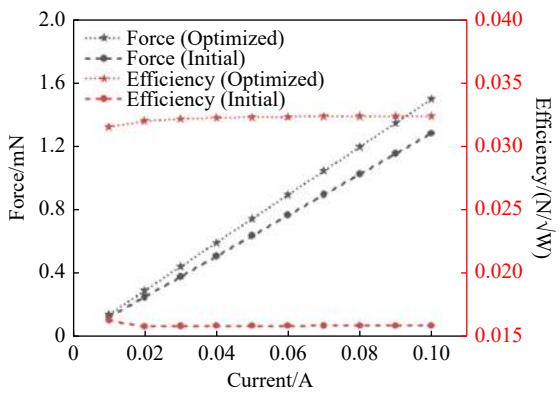

Fig. 6　Electromagnetic force and efficiency as a function of current (Circle line, before optimization; pentagram line, after optimization)

4　Discussions

4.1　Aberration of the thin mirror due to the thermal effect

To investigate the effect of temperature increases from the current in VCAs on the thin mirror, the model of a VCA is analyzed using Maxwell and steady-state thermal modules in Ansys software. The procedure of thermal analysis is shown in Fig.7 (color online).

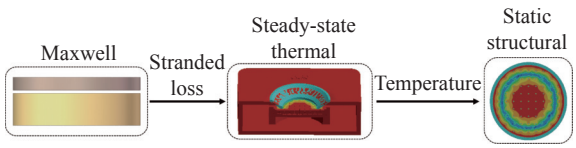

Fig. 7　The thermal analysis process of the VCDM

In compact DMs, active cooling elements such as air cooling and water cooling are generally not used. The thermal convection of all parts in the VCDM is through the air. In the ANSYS steady-state thermal module, the air convection heat transfer coefficient is set to 5 W/(m^{2}K)[23]. According to the mechanical model of the VCDM, as shown in Fig.2, the internal heat generation of the voice coil is introduced by the ohmic loss calculated by the Maxwell module. After that, the thin mirror temperature obtained by the steady-state thermal module is transferred to the static structural module to calculate the thermal deformation of the thin mirror.

The mirror material is CP1 Polyimide from NeXolve[24]. O-rings, springs, and struts are made of 316 Stainless Steel. The adhesive between the struts and the mirror is Epoxy. The material of the permanent magnet is NdFe35, and the material of the coil is copper. To accelerate heat dissipation, the shell of the DM, spring fixing plate, and baseplate are all made of aluminum alloy. The parameters of the adopted materials are listed in Tab. 2.

Fig.8(a) (color online) shows the temperature of the VCDM's thin mirror as a function of currents. The maximum temperature of the mirror surface increases along with the current. When the current

Tab. 2 Material parameters uesd in thermal analysis

Material	Thermal conductivity [W/m/ °C]	Coefficient of thermal expansion [/ °C]	Density [kg/m³]	Young's Modulus [Pa]	Poisson's Ratio [/]
CP1 Polyimide	0.25	5.1×10^{-5}	1540	2.1×10^{9}	0.34
316 Stainless Steel	13.44	1.478×10^{-5}	7954	1.95×10^{11}	0.25
Epoxy	0.294	1.688×10^{-5}	1900	2.64×10^{10}	0.1543
NdFe35	7.7	3.2×10^{-6}	7450	1.6×10^{8}	0.24
Copper	112.1	1.999×10^{-5}	8267	9.995×10^{10}	0.345
Aluminum Alloy	114	2.3×10^{-5}	2770	7.1×10^{10}	0.33

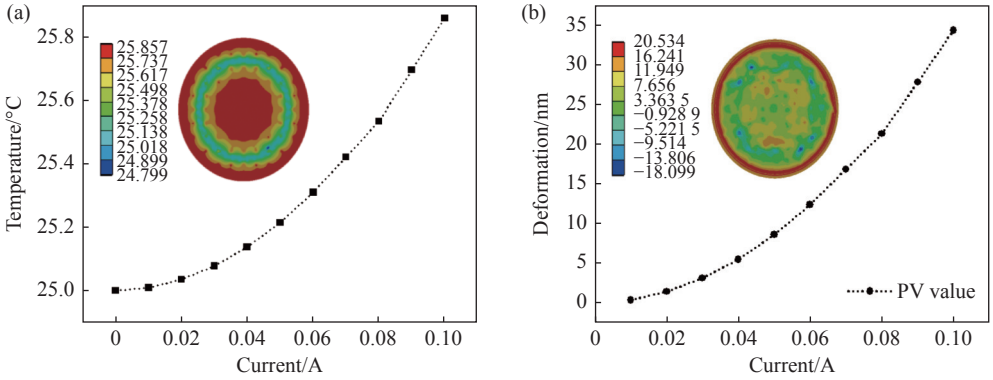

Fig. 8 Temperature and thermal deformation of the VCDM's thin mirror as a function of current. (a) The temperature of the thin mirror as a function of current. The inset shows the temperature chart of the thin mirror when the current is 0.1 A. (b) The thermal deformation chart of the mirror surface as a function of current. The inset shows the deformation chart of the thin mirror when the current is 0.06 A

is 0.1 A corresponding to a current density of 10 A/mm^2, the temperature rise of the VCDM is about 1 degree Celsius. Fig.8(b) (color online) shows the thermal deformation of the thin mirror due to non-uniform distribution of rising temperatures. It indicates that the PV of the thin mirror deformation increases along with the current. When the current density is 6 A/mm^2 corresponding to 0.06 A, the PV is 12.36 nm, which is about 0.022λ for λ=550 nm. Therefore, the maximum control current of a single VCA should not be larger than 0.06 A for good thermal stability. At this time, the temperature and the deformation of the thin mirror are shown in the inserted figures of Fig.8(a) and Fig.8(b).

4.2 First resonance frequency

The first resonance frequency of the VCDM is mainly related to the mirror and the actuator's stiffness. When the mirror material is selected, the mirror's stiffness is determined by its thickness, and the stiffness of the VCA is dominated by the spring. As shown in Fig.9, the first resonance frequency is positively correlated with the spring's stiffness for a given mirror thickness. However, for unchanging spring stiffnesses, the first resonance frequency in-

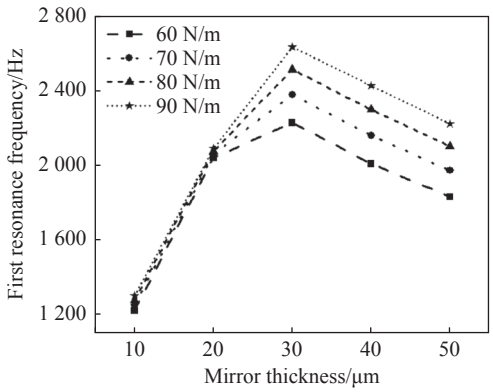

Fig. 9 Relationship between first resonance frequency of the DM and mirror thickness under different spring's stiffnesses

creases and then decreases with an increasing mirror thickness, which shows that there is an extreme point in the relationship. The frame rate of the Adaptive Optics (AO) system should be 10 to 30 times higher than the bandwidth of the closed-loop system. Therefore, a mirror thickness ranging from 20 μm to 50 μm is preferable.

4.3　Wavefront fitting precision

The wavefront fitting precision of the VCDM is important for AO wavefront correction. The influence function of the VCDM could also be expressed as[25]:

$$Z(r) = k \times \exp\left[\ln(\omega) \times \left(\frac{r}{d_0}\right)^{\alpha}\right] \quad , \qquad (7)$$

where $Z(r)$ is the thin mirror deformation at a distance of r, k is the deformation of the mirror at the position of the central actuator, ω is the coupling coefficient that indicating the influence of the central actuator on neighboring actuators, the actuator spacing d_0 is 2.5 mm, and α is the Gaussian index.

The coupling coefficient ω, a key indicator of the DM, is mainly influenced by the thickness of the mirror and the stiffness of the actuator. There is an optimal range of coupling coefficients for a given DM; too large or too small will affect the performance of the system[26]. As shown in Fig.10, the coupling coefficient increases with mirror thickness. In addition, the larger the stiffness, the smaller the coupling coefficient.

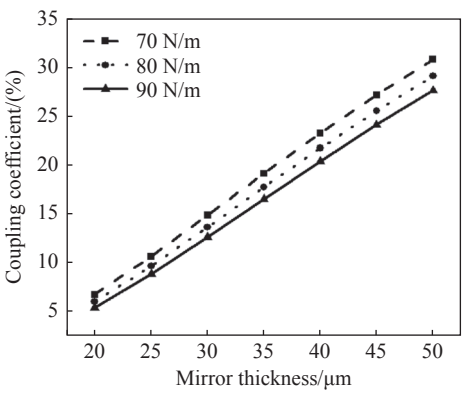

Fig. 10　Relationship between coupling coefficient of the DM and mirror thickness under different spring's stiffnesses

The wavefront fitting errors as a function of the coupling coefficient are shown in Fig.11 for four Zernike modes Z1, Z3, Z6, and Z10 with a PV value of 8 μm. The results indicate that with an increase in the coupling coefficient, errors decrease rapidly at first and then increase slowly. The optimal coupling coefficient for the compact VCDM is about 25%, which is much smaller than that of a standard VCDM with a value larger than 60%. Generally, a relatively low coupling coefficient is preferable for high wavefront correction precision. A VCDM model named S1 with a mirror thickness of 50 μm and an actuator stiffness of 90 N/m was built. Its influence function is shown in Fig.12. Sixty-nine VCAs are arranged in a square array under the thin mirror. The pitch of S1 is 2.5 mm, the coupling coefficient is 24.9% and the first resonance frequency is 2 220 Hz.

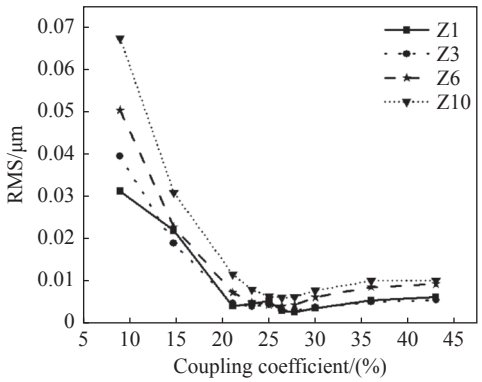

Fig. 11　Correction ability varying with the coupling coefficient

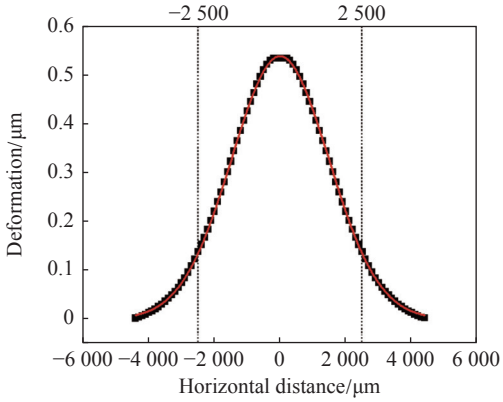

Fig. 12　The influence function of S1

The MATLAB codes were programmed to complete the wavefront fitting and residual calculation according to the influence functions. It should

be pointed out that, to simplify the calculation model, the error caused by thermal deformation and response delay is not considered. In the fitting experiment, S1 is actuated to generate Zernike shapes with a PV value of 1 μm. Fig.13 shows the wavefront Root Mean Square (RMS) of the first 35 Zernike modes and the residual wavefront RMS after fitting. The results indicate that the fitting effect of S1 for the first 35 Zernike modes is very good and the RMS is always less than 30 nm. Compared with the large 121-element VCDM designed by Zhang Z G, the wavefront fitting precision of S1 is higher by 15%[27]. Fig.14 (color online) shows the wavefront fitting results of S1 for a complex random aberration. The complex random aberration consists of 90 Zernike modes and its PV value is 1.647 μm. It can be seen that the fitting wavefront generated by S1 is very similar to the original wavefront. The VCDM S1 reduces the RMS of the complex random aberration from 0.272 2 μm to 0.023 9 μm. The above results show that S1 has high wavefront fitting precision.

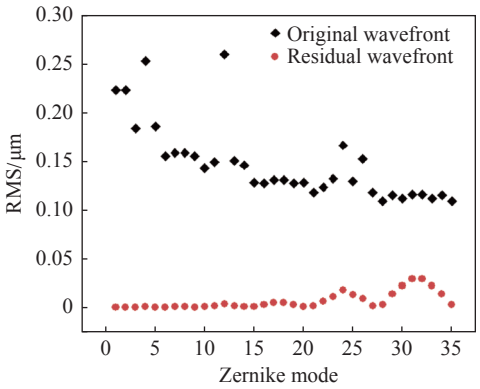

Fig. 13 Wavefront fitting results of S1 for a single Zernike mode

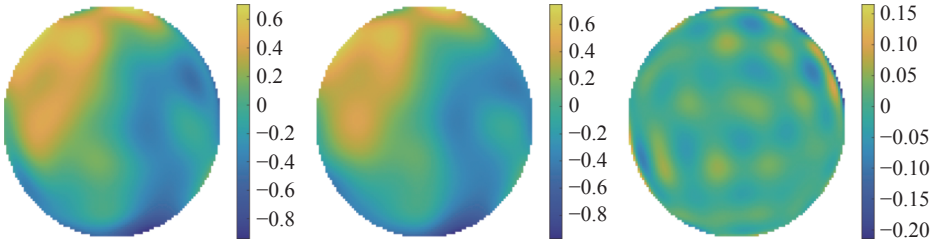

Fig. 14 The wavefront fitting results of S1 for complex random aberrations. From left to right, there is the original wavefront, the fitting wavefront and the residual wavefront

5 Conclusion

The VCDM has many merits, such as being hysteresis-free, requiring low voltage, having a large phase stroke and so on. However, there are many limitations and factors in VCDMs that will affect their performance. In the paper, to design a compact VCDM with improved properties, an analytical expression based on electromagnetic theory is systematically built, which includes its parameters such as phase stroke, force, efficiency, and frequency. They guide the design and reasonable optimization of the compact VCDM. The thin mirror of the VCDM is made of polyimide and is coated with a thin layer of evaporated aluminum in order to make it optically reflective. The struts of micro VCAs are installed in the spring fixing plate, whose springs provide micro VCAs with axial stiffness. This structure makes it possible for the VCDM to have a higher operating bandwidth. Based on multiparameter analysis and finite element analysis using ANSYS, a well-optimized VCDM is obtained with a micro VCA of 2 mm in diameter and an efficiency of 0.032 N/√W. The maximum current of a micro VCA is 0.06 A, which gives the VCDM excellent thermal stability. The temperature difference of the thin mirror is less than 0.4 °C at the maximum current of 0.06 A, and the thermal deformation of the thin mirror is only 12.36 nm. The first resonance frequency of the 69-element compact VCDM S1 is 2 220 Hz. High wavefront fitting precision with a relatively low coupling coefficient of about 25% is also demonstrated in this paper. The fitting results

of Zernike aberrations show that the wavefront fitting precision of the compact VCDM increased by 15% compared with traditional VCDM. In addition, S1 can reduce the wavefront RMS of complex random aberrations to less than 10%. The above results indicate that the compact VCDM can satisfy the requirements of miniaturized adaptive optics systems. The design and optimization methods are also valuable for the design of other kinds of DMs. Our design decreases the development cost of VCDMs and obtains a compact version with high electro-optical performance.

References:

[1] 胡立发, 刘超, 申文, 等. 自适应光学技术在天文观测中的研究进展[J]. 中国科学: 物理学 力学 天文学, 2017, 47(8): 084202.
HU L F, LIU CH, SHEN W, *et al*.. Advancement of adaptive optics in astronomical observation[J]. *Scientia Sinica Physica, Mechanica & Astronomica*, 2017, 47(8): 084202. (in Chinese).

[2] 袁德波, 许亮, 张文斌, 等. 同步辐射用 36 单元压电变形镜研制及其面形调控研究[J]. 中国光学, 2021, 14(6): 1362-1367.
YUAN D B, XU L, ZHANG W B, *et al*.. Development of a 36-element piezoelectric deformable mirror for synchrotron radiation and its surface control ability[J]. *Chinese Optics*, 2021, 14(6): 1362-1367. (in Chinese).

[3] WU ZH ZH, ZHANG T Y, MBEMBA D, *et al*.. Wavefront sensorless aberration correction with magnetic fluid deformable mirror for laser focus control in optical tweezer system[J]. *IEEE Transactions on Magnetics*, 2021, 57(1): 1-6.

[4] KAMEL A, KOCER S, MUKHANGALIYEVA L, *et al*.. Resonant adaptive MEMS mirror[J]. *Actuators*, 2022, 11(8): 224.

[5] 刘新宇, 曹朔, 胡栋挺, 等. 音圈变形镜的设计及其力学特性分析[J]. 液晶与显示, 2020, 35(8): 801-807.
LIU X Y, CAO SH, HU D T, *et al*.. Design of voice-coil deformable mirror and its mechanical characteristics[J]. *Chinese Journal of Liquid Crystals and Displays*, 2020, 35(8): 801-807. (in Chinese).

[6] ANDERSEN T, GARPINGER O, OWNER-PETESEN M, *et al*.. Novel concept for large deformable mirrors[J]. *Optical Engineering*, 2006, 45(7): 073001.

[7] BRUSA G, RICCARDI A, SALINARI P, *et al*.. MMT adaptive secondary: performance evaluation and field testing[J]. *Proceedings of SPIE*, 2003, 4839: 691-702.

[8] BRIGUGLIO R, QUIRÓS-PACHECO F, MALES J R, *et al*.. Optical calibration and performance of the adaptive secondary mirror at the Magellan telescope[J]. *Scientific Reports*, 2018, 8(1): 10835.

[9] WRIGHT T, SPARKS H, PATERSON C, *et al*.. Video-rate remote refocusing through continuous oscillation of a membrane deformable mirror[J]. *Journal of Physics:Photonics*, 2021, 3(4): 045004.

[10] MORGAN R E, DOUGLAS E S, ALLAN G W, *et al*.. MEMS deformable mirrors for space-based high-contrast imaging[J]. *Micromachines*, 2019, 10(6): 366.

[11] FERNANDEZ E J, VABRE L, HERMANN B, *et al*.. Adaptive optics with a magnetic deformable mirror: applications in the human eye[J]. *Optics Express*, 2006, 14(20): 8900-8917.

[12] ZAMKOTSIAN F, LIOTARD A, LANZONI P, *et al*.. Electrostatic micro-deformable mirror for adaptive optics[J]. *Proceedings of SPIE*, 2006, 6272: 627222.

[13] 刘磊, 郭劲, 赵帅, 等. 随机并行梯度下降算法在激光束整形中的应用[J]. 中国光学, 2014, 7(2): 260-266.
LIU L, GUO J, ZHAO SH, *et al*.. Application of stochastic parallel gradient descent algorithm in laser beam shaping[J]. *Chinese Optics*, 2014, 7(2): 260-266. (in Chinese).

[14] NOLL R J. Zernike polynomials and atmospheric turbulence[J]. *Journal of the Optical Society of America*, 1976, 66(3): 207-211.

[15] HARDY J W, THOMPSON L. Adaptive optics for astronomical telescopes[J]. *Physics Today*, 2000, 53(4): 69.

[16] HAMELINCK R F M M. *Adaptive deformable mirror: based on electromagnetic actuators*[D]. Eindhoven: Technische Universiteit Eindhoven, 2010: 23-25.

[17] DOBLE N, MILLER D T, YOON G, *et al*.. Requirements for discrete actuator and segmented wavefront correctors for aberration compensation in two large populations of human eyes[J]. *Applied Optics*, 2007, 46(20): 4501-4514.

[18] ZHAO J L, XIAO F, KANG J, *et al*.. Statistical analysis of ocular monochromatic aberrations in Chinese population for

adaptive optics ophthalmoscope design[J]. *Journal of Innovative Optical Health Sciences*, 2017, 10(1): 1650038.

[19] JAROSZ J, MECÊ P, CONAN J M, *et al*.. High temporal resolution aberrometry in a 50-eye population and implications for adaptive optics error budget[J]. *Biomedical Optics Express*, 2017, 8(4): 2088-2105.

[20] WANG CH CH, LU SH ZH, ZHANG C Y, *et al*.. Design and dynamic modeling of a 3-RPS compliant parallel robot driven by voice coil actuators[J]. *Micromachines*, 2021, 12(12): 1442.

[21] 张志高, 胡启立, 马文超, 等. 高效率可变磁阻音圈驱动器的设计及性能研究[J]. 液晶与显示, 2022, 37(1): 21-28.
ZHANG ZH G, HU Q L, MA W CH, *et al*.. Design and performance research of high efficiency variable reluctance voice coil actuator[J]. *Chinese Journal of Liquid Crystals and Displays*, 2022, 37(1): 21-28. (in Chinese).

[22] CUGAT O, BASROUR S, DIVOUX C, *et al*.. Deformable magnetic mirror for adaptive optics: technological aspects[J]. *Sensors and Actuators A:Physical*, 2001, 89(1-2): 1-9.

[23] BANERJEE K, RAJAEIPOUR P, ZAPPE H, *et al*.. A 37-actuator polyimide deformable mirror with electrostatic actuation for adaptive optics microscopy[J]. *Journal of Micromechanics and Microengineering*, 2019, 29(8): 085005.

[24] YU E, JOSHI Y K. Natural convection air cooling of electronic components in partially open compact horizontal enclosures[J]. *IEEE Transactions on Components and Packaging Technologies*, 2000, 23(1): 14-22.

[25] HUANG L H, RAO CH H, JIANG W H. Modified Gaussian influence function of deformable mirror actuators[J]. *Optics Express*, 2008, 16(1): 108-114.

[26] AHN K, KIHM H. Moment actuator for correcting low-order aberrations of deformable mirrors[J]. *Optics and Lasers in Engineering*, 2020, 126: 105864.

[27] 张志高. 模块化音圈变形镜的结构设计与性能研究[D]. 无锡: 江南大学, 2022.
ZHANG ZH G. *Structure design and performance research of modular voice coil deformable mirror*[D]. Wuxi: Jiangnan University, 2022. (in Chinese).

Author Biographics:

HU Li-fa (1974—), male, born in Wuhan, Hubei Province, Ph.D., researcher and doctoral supervisor, obtained a doctorate degree from Northeastern University in 2003, is mainly engaged in liquid crystal adaptive optics research. E-mail: hulifa@jiangnan.edu.cn

HUANG Yang (1988—), male, born in Nantong, Jiangsu Province, Ph.D., associate professor and master supervisor, obtained a doctorate degree from Soochow University in 2016, is mainly engaged in adaptive optics technology and application research. E-mail: yanghuang@jiangnan.edu.cn